# Influence of Carbon Black on Decompression Failure and Hydrogen Permeation Properties of Filled Ethylene-Propylene–Diene–Methylene Rubbers Exposed to High-Pressure Hydrogen Gas

**Junichiro Yamabe,[1,2] Shin Nishimura[2,3]**

[1]*Hydrogen Safety Engineering Division, International Research Center for Hydrogen Energy, Kyushu University, Fukuoka 819-0395, Japan*
[2]*Research Center for Hydrogen Industrial Use and Storage (HYDROGENIUS), National Institute of Advanced Industrial Science and Technology (AIST), Fukuoka 819-0395, Japan*
[3]*Department of Mechanical Engineering, Kyushu University, Fukuoka 819-0395, Japan*

Received 15 December 2010; accepted 13 February 2011
DOI 10.1002/app.34344
Published online 8 July 2011 in Wiley Online Library (wileyonlinelibrary.com).

**ABSTRACT:** Eight carbon black (CB)-filled ethylene–propylene–diene–methylene linkage (EPDM) rubbers were manufactured by varying the content and type of CB. Then, the relationship among crack damage caused by high-pressure hydrogen decompression, the hydrogen permeation properties, and the mechanical properties of the rubbers was investigated. The hydrogen gas permeability of the rubbers decreased with an increase in the CB content and depended little on primary particle size. In contrast, the hydrogen gas diffusivity and solubility depended on both the CB content and primary particle size, that is, the hydrogen gas diffusivity decreased with an increase in the CB content and a decrease in the primary particle size, and the hydrogen gas solubility increased with an increase in the CB content and a decrease in the primary particle size. As for the mechanical properties, the CB-filled rubbers were more strongly reinforced by an increase in the CB content and a decrease in the primary particle size. The crack damage by high-pressure hydrogen decompression became larger as the ratio of the hydrogen gas solubility to estimated internal pressure at crack initiation relating to the mechanical properties became larger. As a smaller CB particle increases the hydrogen gas solubility of EPDM rubbers, while at the same time it reinforces the rubbers, the crack damage in the CB-filled rubbers was not influenced by the primary particle size. © 2011 Wiley Periodicals, Inc. J Appl Polym Sci 122: 3172–3187, 2011

**Key words:** rubber; elastomers; electron microscopy; decompression failure; hydrogen

## INTRODUCTION

Fuel-cell systems that use energy derived from hydrogen have received a considerable amount of attention recently as a solution to the issue of the exhaustion of fossil fuels and the problems associated with global warming. To achieve widespread acceptance by society of hydrogen-based energy, it is necessary to clarify the influence of hydrogen on the mechanical, physical, and chemical properties of the materials used for hydrogen energy systems. In the case of rubbers, there is a particular danger of mechanical damage resulting from internal fracture, which occurs when high-pressure hydrogen gas is suddenly decompressed. This internal fracture is sometimes referred to as "blister fracture" or "explosive decompression failure.[1]" Although there are several reports on the internal fracture of rubbers caused by high-pressure carbon dioxide, nitrogen, and argon gases,[1–10] there are no reports on internal fractures resulting from high-pressure hydrogen decompression.

In previous studies,[11–15] we clarified that the internal fractures of rubbers have occurred as a result of high-pressure hydrogen decompression, and we estimated the hydrogen pressure at crack initiation in terms of fracture mechanics under the assumption that submicrometer-sized bubbles, which are hardly observed using optical microscopy, were formed from dissolved hydrogen molecules after decompression and grew to micrometer-size with the elapse of time after decompression; consequently, micrometer-sized cracks were initiated due to the stress concentration of the bubbles. Experimental data were successfully estimated under this assumption. In this investigation, a bubble is defined as a submicrometer-size cavity that can hardly be observed using optical microscopy. It is considered that as a rubber often contains micrometer-sized defects in its structure, the bubble has little influence

*Correspondence to:* J. Yamabe (yamabe@mech.kyushu-u.ac.jp).


© 2011 Wiley Periodicals, Inc.

**TABLE I**
**Physicochemical Properties of Carbon Black Particles**

| Items | Carbon black (CB) | | | | |
|---|---|---|---|---|---|
| | N110 | N220 | N330 | N550 | N774 |
| Primary particle size (nm) | 19 | 22 | 28 | 43 | 66 |
| $N_2$ specific surface area ($m^2/g$) | 142 | 119 | 79 | 42 | 27 |
| Iodine absorption value (mg/g) | 139 | 121 | 80 | 44 | 26 |
| Dibutyl phtalate (DBP) absorption value ($cm^3/100$ g) | 115 | 114 | 101 | 115 | 68 |
| Pour density ($kg/m^3$) | 370 | 330 | 380 | 380 | 520 |

on the macroscopic mechanical properties of the rubber, such as tensile elastic modulus and tensile strength, unless the bubble grows and causes crack initiation. From this viewpoint, a bubble is regarded as a mechanically reversible cavity, while a crack is a mechanically irreversible cavity. The nanoscale fracture caused by a submicrometer-sized bubble is confirmed in terms of the measurement of acoustic emission.

Cylindrical specimens ($\phi$ 29.0 $\times$ 12.5 $mm^2$) made of ethylene–propylene–diene–methylene (EPDM) and acrylonitrile–butadiene rubber filled with carbon black (CB) (ASTM N330) and silica (SC) were also exposed to hydrogen gas at pressures of up to 10 MPa, and the effects of the strength properties and the hydrogen concentrations of the rubbers on their internal fracture behavior were examined.[14] As a result, it was clarified that the crack damage of the rubbers became slighter with a decrease in their hydrogen concentration (hydrogen gas solubility) and an increase in their tensile elastic modulus and tensile strength. As CB raises the hydrogen concentration of the rubbers different from SC, the crack damage of the CB-filled rubbers was more serious than that of SC-filled rubbers.

In this study, five types of CB (ASTM N110, N220, N330, N550, and N744) were selected, and eight filled EPDM rubbers were manufactured by varying the contents and type of CB used. Hydrogen permeation and high-pressure hydrogen exposure tests of the filled rubbers were conducted; then, the influence of the CB type on the hydrogen permeation properties and crack damage was investigated.

## EXPERIMENTAL

### Materials

The fuel-cell systems were planned to be operated under a wide range of ambient temperatures. Therefore, heat resistance and low-temperature properties are demanded for the sealing rubber of the fuel-cell systems in addition to the resistance for internal fracture. From the viewpoint of the heat resistance and low-temperature properties, EPDM rubber was used as a base polymer. This study used eight types of CB-filled sulfur-vulcanized EPDM rubbers. These rubbers were manufactured by Takaishi-Industy Co., ltd (Osaka, Japan). Table I shows the physicochemical properties of the CBs used in this study.[16]. Five types of CB with a different primary particle size were used (ASTM N110, N220, N330, N550 and N774). The primary particle size decreases with an increase in $N_2$ surface area. Table II shows the material compound, density, and hardness of the rubbers. The compounds of the rubbers used in our previous study (NF, SC-30, SC-60, NFP, SCP, and CBP) are also shown in Table II.[13,14] While NF is unfilled, SC-30 and SC-60 are SC-filled. Wet SC (Nippon Silica Co., NIPSIL VN3) was used, which has a reported primary particle size and $N_2$ specific surface area of 16 nm and 240 $m^2/g$, respectively.[17] unfilled and peroxide-crosslinked EPDM (NFP), SC-filled and peroxide-crosslinked EPDM (SCP), and CB-filled and peroxide-crosslinked EPDM (CBP) were crosslinked by peroxide, and the critical hydrogen pressures at crack initiation were quantitatively evaluated in terms of fracture mechanics in our previous study.[13] The CB was compounded with EPDM in a weight ratio of 50 : 100 or in a weight ratio of 25 : 100. For example, these CB-filled rubbers are referred to as N110-50 and N110-25. The volume fraction of the 50 phr CB-filled rubbers was the same as that of SC-60. A sheet specimen with a thickness of 2.0 mm, and a cylindrical specimen with a diameter of 29.0 mm and a thickness of 12.5 mm were manufactured from the rubbers. The EPDM rubber used in this study was Esprene 505. The mastication and mixing of its rubber were conducted by using an 18-inch two-roll mill. First, the mastication of the rubber was conducted for 10 min. Then, filler, zinc oxide, sulfur, stearic acid and vulcanization accelerators were added to the masticated rubber; afterward, these were mixed for 10–15 min. The added amount of these chemical additives is shown in Table II. Dibenzothiazyl disulfide (MBTS), tetramethylthiuram disulfide (TMTD), and zinc diethyldithiocarbamate (ZnEDC) were used as the vulcanization accelerators. The compounded rubber obtained by mixing was molded and vulcanized under the pressure of 15 MPa. The vulcanization of the sheet specimen was conducted at 170°C for 10 min, while that of the cylindrical specimen was conducted at 150°C for 30 min.

**TABLE II**
**Material Composition (Parts By Weight Per Hundred Parts of Rubber: phr), Density and Hardness of Rubbers**

| Items | N110–25 | N220–25 | N330–25 | N550–25 | N774–25 | N110–50 | N330–50 | N774–50 | NF | SC-30 | SC-60 | NFP | SCP | CBP |
|---|---|---|---|---|---|---|---|---|---|---|---|---|---|---|
| EPDM | 100 | 100 | 100 | 100 | 100 | 100 | 100 | 100 | 100 | 100 | 100 | 100 | 100 | 100 |
| Stearic acid | 1.0 | 1.0 | 1.0 | 1.0 | 1.0 | 1.0 | 1.0 | 1.0 | 1.0 | 1.0 | 1.0 | – | – | – |
| Zinc oxide | 5.0 | 5.0 | 5.0 | 5.0 | 5.0 | 5.0 | 5.0 | 5.0 | 5.0 | 5.0 | 5.0 | – | – | – |
| Sulfur | 1.5 | 1.5 | 1.5 | 1.5 | 1.5 | 1.5 | 1.5 | 1.5 | 1.5 | 1.5 | 1.5 | – | – | – |
| MBTS[a] | 1.5 | 1.5 | 1.5 | 1.5 | 1.5 | 1.5 | 1.5 | 1.5 | 1.5 | 1.5 | 1.5 | – | – | – |
| TMTD[a] | 0.7 | 0.7 | 0.7 | 0.7 | 0.7 | 0.7 | 0.7 | 0.7 | 0.7 | 0.7 | 0.7 | – | – | – |
| ZnEDC[a] | 0.7 | 0.7 | 0.7 | 0.7 | 0.7 | 0.7 | 0.7 | 0.7 | 0.7 | 0.7 | 0.7 | – | – | – |
| 1,3,5-Triallylisocyanurate | – | – | – | – | – | – | – | – | – | – | – | 1.0 | 1.0 | 1.0 |
| Dicumyl peroxide | – | – | – | – | – | – | – | – | – | – | – | 2.5 | 2.5 | 2.5 |
| Vinyl tris(β-methoxyethoxy) silane | – | – | – | – | – | – | – | – | – | – | – | – | 1.0 | – |
| Carbon black | | | | | | | | | | | | | | |
| N110 | 25 | – | – | – | – | 50 | – | – | – | – | – | – | – | – |
| N220 | – | 25 | | – | – | – | – | – | – | – | – | – | – | – |
| N330 | – | – | 25 | – | – | — | 50 | – | – | – | – | – | – | 56 |
| N550 | – | – | – | 25 | – | – | – | – | – | – | – | – | – | – |
| N774 | – | – | – | – | 25 | – | – | 50 | – | – | – | – | – | – |
| Silica | – | – | – | – | – | – | – | – | – | 30 | 60 | – | 40 | – |
| Density (g/cm$^3$) | 1.015 | 1.014 | 1.016 | 1.017 | 1.014 | 1.093 | 1.093 | 1.093 | 0.928 | 1.039 | 1.136 | 0.857 | 1.037 | 1.061 |
| Hardness | A69 | A69 | A68 | A68 | A66 | A81 | A79 | A72 | A54 | A71 | A91 | A 52 | A 77 | A 77 |

[a] MBTS: dibenzothiazyl disulfide, TMTD: tetramethylthiuram disulfide, ZnEDC: zinc diethyldithiocarbamate.

## Specimen and experimental method

### Tensile and compressive tests

A type-1 dumbbell specimen (JIS K 6251) was obtained from the sheet specimen. A tensile tester (Shimadzu Corp., Autograph AG-X) was used in the experiments. The specimen was elongated under atmospheric pressure (0.1 MPa) at room temperature (20–25°C) under the condition that the relationship between cross-head speed ($d'$) and the distance of chucking digs ($d$) meets $d'/d \approx 0.8/\text{min}$, as the relationship between nominal stress and nominal strain of rubber materials generally depends on the cross-head speed. The influence of CB on the tensile properties of the CB-filled rubbers was examined by this tensile test. A compressive test (JIS K6254) was also conducted using the cylindrical specimen ($\phi$ 29.0 $\times$12.5 mm-) under the condition that meets $d'/d \approx 0.8/\text{min}$. Two specimens were tested for the tensile and compressive tests for each rubber. For stress analysis, the rubbers were regarded as hyperelastic materials with the strain energy function as follows:

$$W_0(I_1, I_2) = C_{10}(I_1 - 3) + C_{01}(I_2 - 3) + C_{20}(I_1 - 3)^2 \quad (1)$$

where $W_0(I_1, I_2)$ is the strain energy function; $I_1$, $I_2$ the first and second invariants of deformation; and $C_{10}$, $C_{01}$, $C_{20}$ are the material constants. The model expressed by eq. (1) is referred to as a polynominal Mooney–Rivlin model.[18] For monotonic tension and compression, the invariants of $I_1$ and $I_2$ can be written as follows:

$$I_1 = \lambda^2 + \frac{2}{\lambda}; \quad I_2 = 2\lambda + \frac{1}{\lambda^2}, \quad (2)$$

where $\lambda$ is the stretch ratio. The nominal stress ($\sigma_n$) in the direction to tension and compression is expressed as follows:

$$\sigma_n = \frac{dW_0(\lambda)}{d\lambda} = 2(\lambda - \frac{1}{\lambda^2})[C_{10} + \frac{C_{01}}{\lambda} + 2C_{20}(\lambda^2 + \frac{2}{\lambda} - 3)] \quad (3)$$

The nominal stress–strain curves obtained from two specimens were nearly equal except for their tensile strength. Therefore, eq. (3) was fitted to the experimental nominal stress–stretch curves of tensile and compressive tests with higher tensile strength by the least square method; then, the material constants ($C_{10}$, $C_{01}$, $C_{20}$) were estimated.

### Observation by atomic force microscopy of filler distribution in rubbers

To confirm the distribution of filler in a rubber structure, observation by atomic force microscopy (AFM) (Veeco Dimension 3100 / Nanoscope V) was conducted. A cantilever with a spring constant and tip radius of 40 N/m and <10 nm (nominal values), respectively, was used, and the observation was conducted under intermitted contact mode (tapping mode) at a drive frequency of 300 kHz. The surface of specimens was finished by a cryomicrotome (Leica Microsystems, EM FC6).

### Hydrogen and nitrogen absorption tests of filler particles

Hydrogen and nitrogen absorbed by filler particles were measured using an automatic gas adsorption analyzer (Sysmex Corp., Nova e3200). A constant volume method was used. Absorption of nitrogen and hydrogen was measured at liquid nitrogen temperature. In general, the nitrogen absorption follows the BET adsorption isotherm[19]:

$$n = \frac{vn_m x}{(1-x)(1-x+vx)}; \quad x = \frac{p}{p_0}, \quad (4)$$

where $p$ and $p_0$ are the equilibrium and the saturation pressures of adsorbates at the temperature of adsorption, $n$ is the adsorbed gas amount, and $n_m$ is the monolayer adsorbed gas amount, $v$ is the BET constant.

### Hydrogen permeation tests of rubbers

The hydrogen permeation properties of the rubbers were measured using a hydrogen permeation tester (GTR Tec Corp., GTR-30AFKU). Hydrogen gas that permeates a thick sheet specimen with a thickness of 2 mm was measured under a differential pressure of 0.6 MPa. When the hydrogen concentration at the high-pressure side is $c_1$ and that at the low-pressure side is zero, the amount of hydrogen gas that permeates the specimen ($q$) can be written under a steady condition as follows[20]:

$$q = \frac{DAc_1}{l}(t - \frac{l^2}{6D}) \quad (5)$$

where $D$ is the hydrogen gas diffusivity, $A$ permeation area, and $l$ is the thickness of the specimen. According to our previous study,[14] a hydrogen concentration at 10 MPa or less follows Henry's law:

$$c = Sp \quad (6)$$

where $S$ is the hydrogen gas solubility. Therefore, eq. (5) can be written as follows:

$$q = \frac{DAc_1}{l}(t - \frac{l^2}{6D}) = \frac{DSAp_1}{l}(t - \frac{l^2}{6D}) \quad (7)$$

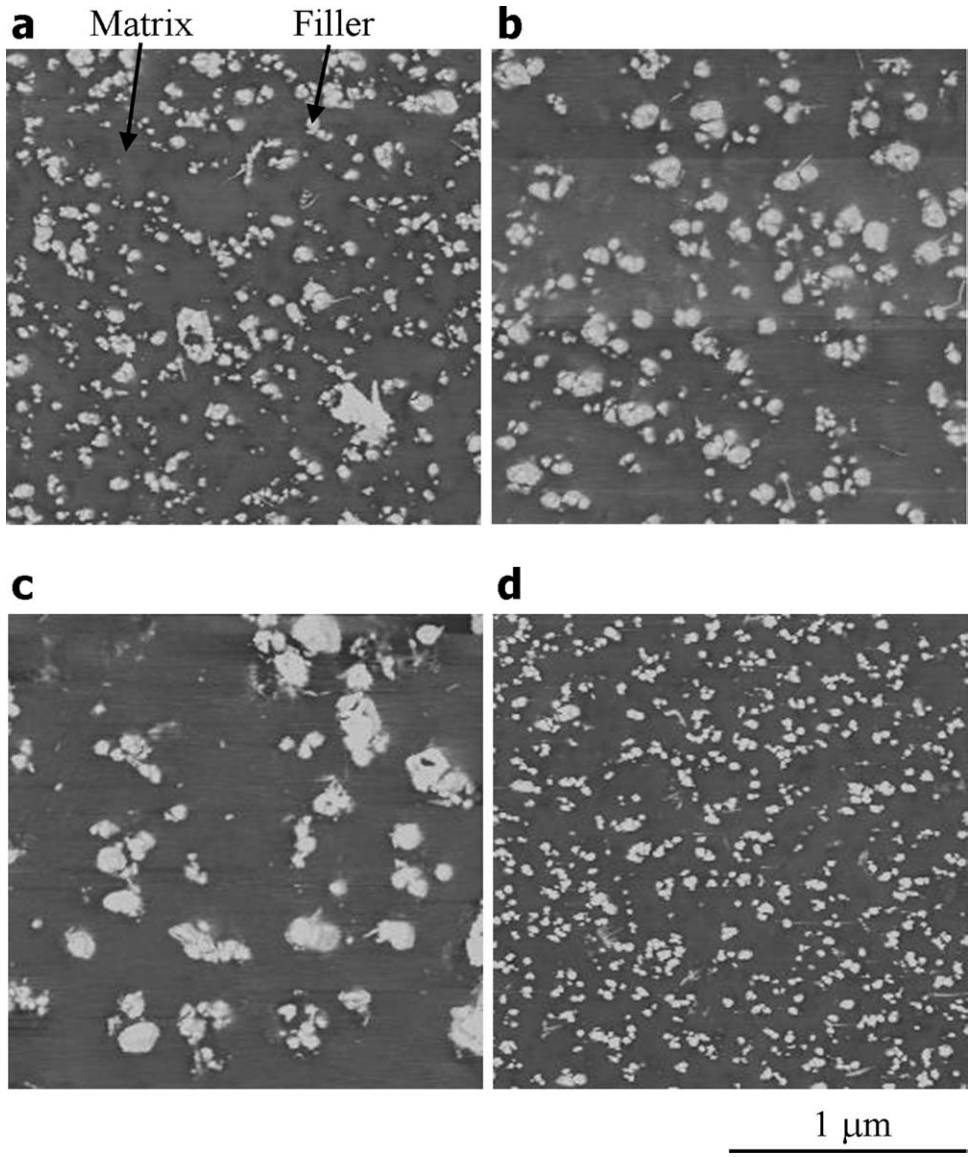


**Figure 1** Phase images of rubber structures by atomic force microscopy: (a) N110-50, (b) N330-50, (c) N774-50, and (d) SC-60.

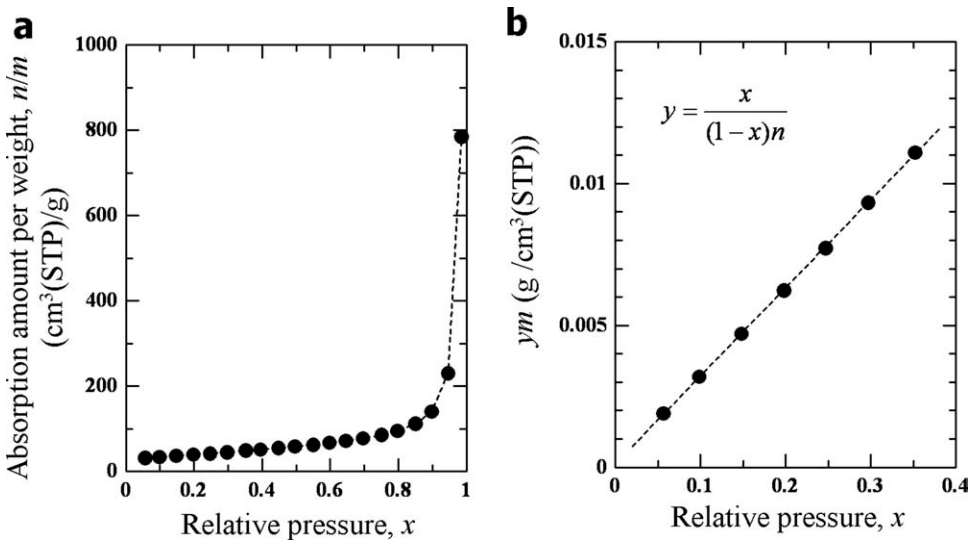


**Figure 2** Nitrogen absorption of carbon black N110 by gas absorption analyzer: (a) relationship between nitrogen absorption and relative pressure, (b) BET plot of nitrogen absorption.

**TABLE III**
**Nitrogen and Hydrogen Absorptions of Carbon Black and Silica Particles**

| Items | Carbon black (CB) | | | | | Silica (SC) |
|---|---|---|---|---|---|---|
| | N110 | N220 | N330 | N550 | N774 | |
| $N_2$ specific surface area ($m^2/g$) | 139 | 124 | 76 | 44 | 30 | 211 |
| $H_2$ absorption amount[a] ($cm^3$ (STP)/g) | 17.9 | 16.4 | 9.0 | 5.5 | 3.7 | 44.9 |

[a] Measured condition: 0.1 MPa and liquid nitrogen temperature.

The hydrogen gas permeability ($Q$), $D$, and $S$ are defined as follows:

$$Q = \frac{q'l}{(Ap_1)}, \text{ where } q' = \frac{dq}{dt}; \qquad D = \frac{l^2}{6t_D}; \quad S = \frac{Q}{D}, \tag{8}$$

where $t_D$ is the time when $q = 0$ in eq. (7) and is referred to as delay time. This measurement was conducted at temperatures ranging from 30 to 70°C; then, one specimen was tested at each temperature.

### Hydrogen exposure tests of rubbers

A cylindrical specimen ($\phi$ 29.0 × 12.5 $mm^2$) was exposed to hydrogen gas at 10 MPa and 30°C for 65 h. Three specimens were tested for each rubber. After decompression, the specimen was kept for 24 h at atmospheric pressure (0.1 MPa) at room temperature (20–25 °C). The specimen was then cut with a cutter, and the crack initiation status on the cross-section was observed using an optical microscopy (Keyence Corp., VHX-900) and scanning electron microscopy (Hitachi High-Technologies Corp., S-4800, and Shimadzu Corp., SS-550).

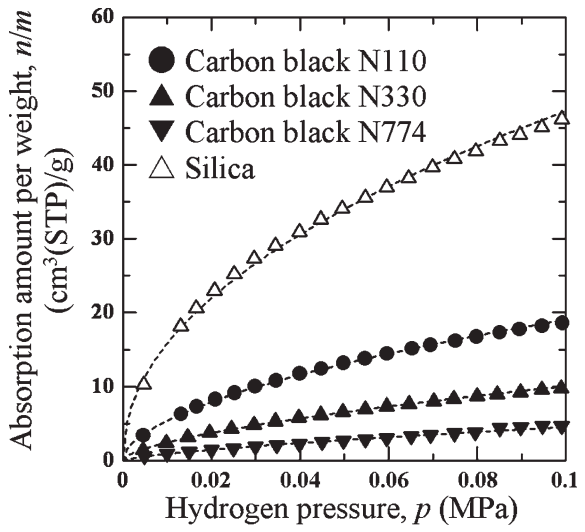


**Figure 3** Relationship between hydrogen absorption and pressure of carbon blacks N110, N330, N774, and silica.

## RESULTS AND DISCUSSION

### Filler distribution in rubbers by atomic force microscopy

Figure 1 shows phase images of rubber structures obtained by AFM, which show images of N110-50, N330-50, N774-50, and SC-60. Several aggregations of filler particles are formed in the rubber structure, as those sizes are somewhat larger than the primary particle sizes mentioned above. Of the rubbers observed by AFM, the filler particles of SC-60 were distributed most finely, while those of N774-50 were distributed most coarsely.

### Hydrogen absorption properties of fillers

Figure 2(a) shows the relationship between the absorption amount and the relative pressure of CB N110 measured under nitrogen gas and liquid nitrogen temperature. In the case of the Brunauer-Emmett-Teller (BET) adsorption isotherm, the following equation from eq. (4) was obtained when $x \approx 1$:

$$n \approx \frac{vn_m x;}{vx(1-x)} = \frac{n_m}{1-x} \to \infty; \quad x \to 1, \tag{9}$$

The nitrogen absorption in Figure 2(a) shows the tendency expressed by eq. (9). Furthermore, eq. (4) can be written as follows:

$$\frac{x}{(1-x)n}(=y) = \frac{1}{vn_m} + \frac{v-1}{vn_m}x \tag{10}$$

Figure 2(b) shows the relationship between $y$ and $x$ of the nitrogen absorption shown in Figure 2(a). The data when $0.05 \leq x \leq 0.30$ are shown. The nitrogen absorption was well reproduced by the BET adsorption isotherm. Table III shows the $N_2$ specific surface areas of CBs (N110, N220, N330, N550, and N774) and SC. The $N_2$ specific surface areas obtained from this study showed a good agreement with the results of reference data.[16,17]

Figure 3 shows the relationship between the absorption amount and the pressure of the CBs (N110, N330, and N774) and SC measured under hydrogen gas at liquid nitrogen temperature. The hydrogen absorption does not follow the BET adsorption isotherm as known from the tendency

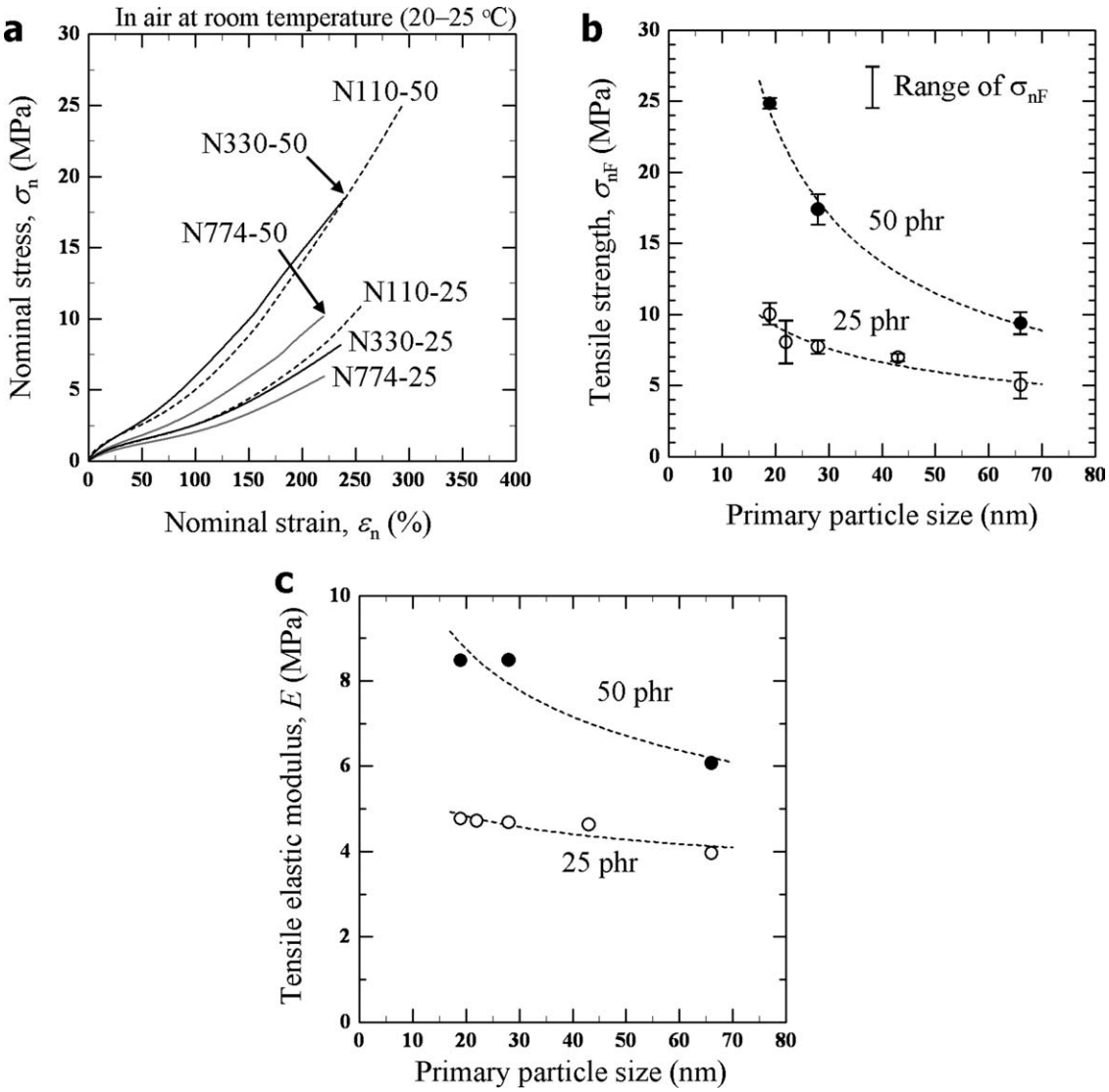


**Figure 4** Tensile properties of CB-filled rubbers: (a) examples of nominal stress–strain curves, (b) relationship between tensile strength and primary particle size, and (c) relationship between tensile elastic modulus and primary particle size.

shown in eq. (9). This is because these measurements were conducted under liquid nitrogen temperature, and it is necessary to conduct measurements at lower than liquid nitrogen temperature to obtain a sufficient absorption amount of hydrogen gas. The hydrogen absorption of the fillers used in this study was fitted using the Freundlich adsorption isotherm[21]:

$$n = ap^{1/u} \tag{11}$$

where $a$ and $u$ are the constants that are independent of pressure. The hydrogen absorption amount of the SC was the largest of all the fillers shown in Figure 3, while that of CB N774 was the smallest. Table III shows the hydrogen absorption amount at a hydrogen pressure of 0.1 MPa and liquid nitrogen temperature. When the $N_2$ specific surface area became larger, the hydrogen absorption amount also became larger.

### Tensile properties of rubbers

Figure 4(a) shows examples of the nominal stress and strain curves ($\sigma_n$–$\varepsilon_n$ curves) of EPDM rubbers (N110-50, N330-50, N774-50, N110-25, N330-25, and N774-25) in air at room temperature (20–25°C). The $\sigma_n$–$\varepsilon_n$ curves of the EPDM rubbers depended on the type and added amount of CB. Figure 4(b) shows the relationship between tensile strength ($\sigma_{nF}$) and primary particle size. When a smaller CB particle was added, the reinforcement effect became higher. Figure 4(c) shows the relationship between tensile elastic modulus ($E$) and primary particle size. Since the $\sigma_n$–$\varepsilon_n$ curves of two specimens were nearly equal except for their tensile strength, the error bars of the tensile elastic modulus are not shown in Figure 4(c). The tensile elastic

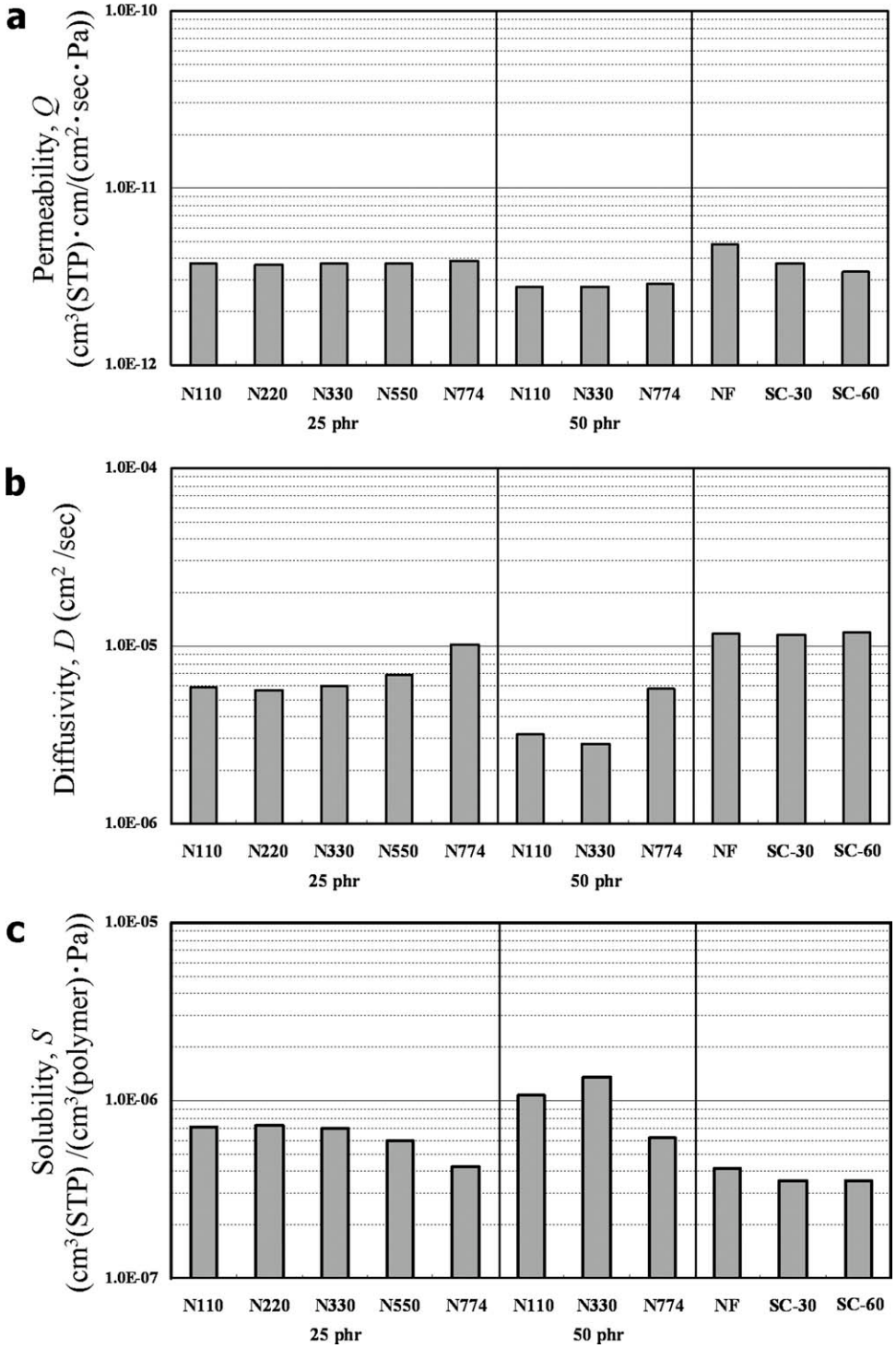


**Figure 5** Hydrogen permeation properties of rubbers under differential pressure of 0.6 MPa and 30° by hydrogen permeation tester: (a) hydrogen gas permeability, (b) hydrogen gas diffusivity, and (c) hydrogen gas solubility.

modulus of the rubbers also showed a tendency to increase with an increase in the CB content.

### Influence of fillers on hydrogen permeation properties of rubbers (30 °C)

Figure 5 shows the hydrogen gas permeability ($Q$), diffusivity ($D$), and solubility ($S$) of rubbers tested at 30°C. The structure of filled rubbers is composed of matrix and filler. Hydrogen gas solubility was based on the volume of the matrix in the rubbers. For the calculation of the solubility, the volume ratio of polymer to filler is assumed to be 90 : 10 for 25 phr CB-filled and 30 phr SC-filled rubbers, and that is assumed to be 80 : 20 for 50 phr CB-filled and 60 phr SC-filled rubbers.

As for hydrogen gas permeability ($Q$), the $Q$ value of NF was the largest of all the rubbers. The $Q$ value became smaller when the filler content became higher, irrespective of the type of filler. Furthermore, as the $Q$ values of the rubbers with the same CB content were nearly equal, it can be said that hydrogen gas permeability was little influenced by the primary particle size ($N_2$ surface area) of the CB.

As for hydrogen gas diffusivity ($D$), the $D$ value as well as the $Q$ value of NF was the largest of all the rubbers. However, the $D$ value became smaller when CB was added, while that hardly changed when SC was added, different from the $Q$ value. From Figure 5(b), the $D$ values depended on the type of CB, and these values became smaller when $N_2$ specific surface area became larger. When filler particles simply act on obstacles for hydrogen diffusion, it is considered that the $D$ value does not depend on the type of CB in the case that the volume fraction is the same. However, the $D$ value depended on the type of CB under the same volume fraction. Our previous study[14] mentioned that solute hydrogen molecules were absorbed at the interface between CB and the matrix in a rubber structure; consequently, the solubility of CB-filled rubbers increased compared with that of unfilled and SC-filled rubbers. When $N_2$ specific surface areas become larger (primary particles become smaller), the number of absorbed hydrogen molecules becomes larger. It is inferred that these absorbed hydrogen molecules participated in hydrogen diffusion; consequently, diffusivity depended on the primary particle size of CBs.

With regard to the hydrogen gas solubility ($S$), the $S$ value increased when CB was added, compared with that of NF. The $S$ values depended on the type of CB as well as the $D$ value. Figure 6 shows the relationship among the diffusivity, primary particle size, and $N_2$ specific surface area of the CB-filled rubbers. The results of 25 phr CB-filled rubbers are shown in Figure 6. The $S$ values of N110-25, N220-25, and N330-25 that were filled with relatively smaller CB particles did not show a big difference. In contrast, the $S$ values of N550-25 and N774-25 that were filled with relatively larger CB particles clearly decreased with a decrease in the $N_2$ specific surface area (an increase in the primary particle size). Especially, the $S$ value of N774-25 was nearly equal to that of NF. The $S$ values of the SC-filled rubbers were nearly equal to that of NF, although the $N_2$ specific surface area and absorbed hydrogen amount of SC were larger than those of CB. This result implies that the CB and SC differ in terms of the interface structure. Therefore, it is believed that the hydrogen gas solubility of filled rubbers is influenced not only by the surface area of fillers but also by the interface structure between filler and matrix.

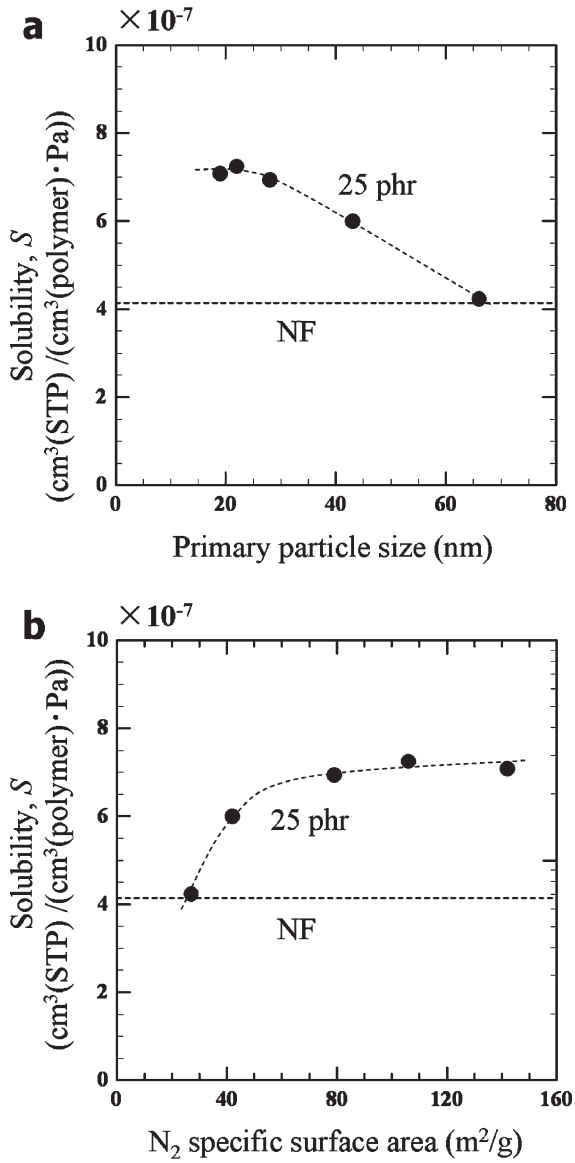


**Figure 6** Influences of primary particle size and specific surface area of nitrogen gas on hydrogen gas solubility of 25 phr CB-filled rubbers: (a) relationship between hydrogen gas solubility and primary particle size and (b) relationship between hydrogen gas solubility and $N_2$ specific surface area.

### Hydrogen exposure tests

Figure 7 shows crack initiation behavior of unfilled, CB-filled and SC-filled rubbers exposed to hydrogen gas at 10 MPa and 30°C for 65 h obtained by optical microscopy. Three specimens were tested by material; the maximum crack area ($A_{max}$) on their cross-sections was measured by specimen, i.e., three $A_{max}$ values are obtained. Cross-sections with the largest $A_{max}$ value, which is indicated by arrows in Figure 7, are shown. Internal cracks can be seen in all the CB-filled rubbers, although the crack damage of these rubbers was slighter than that of NF. The crack damage of the CB-filled rubbers was hardly

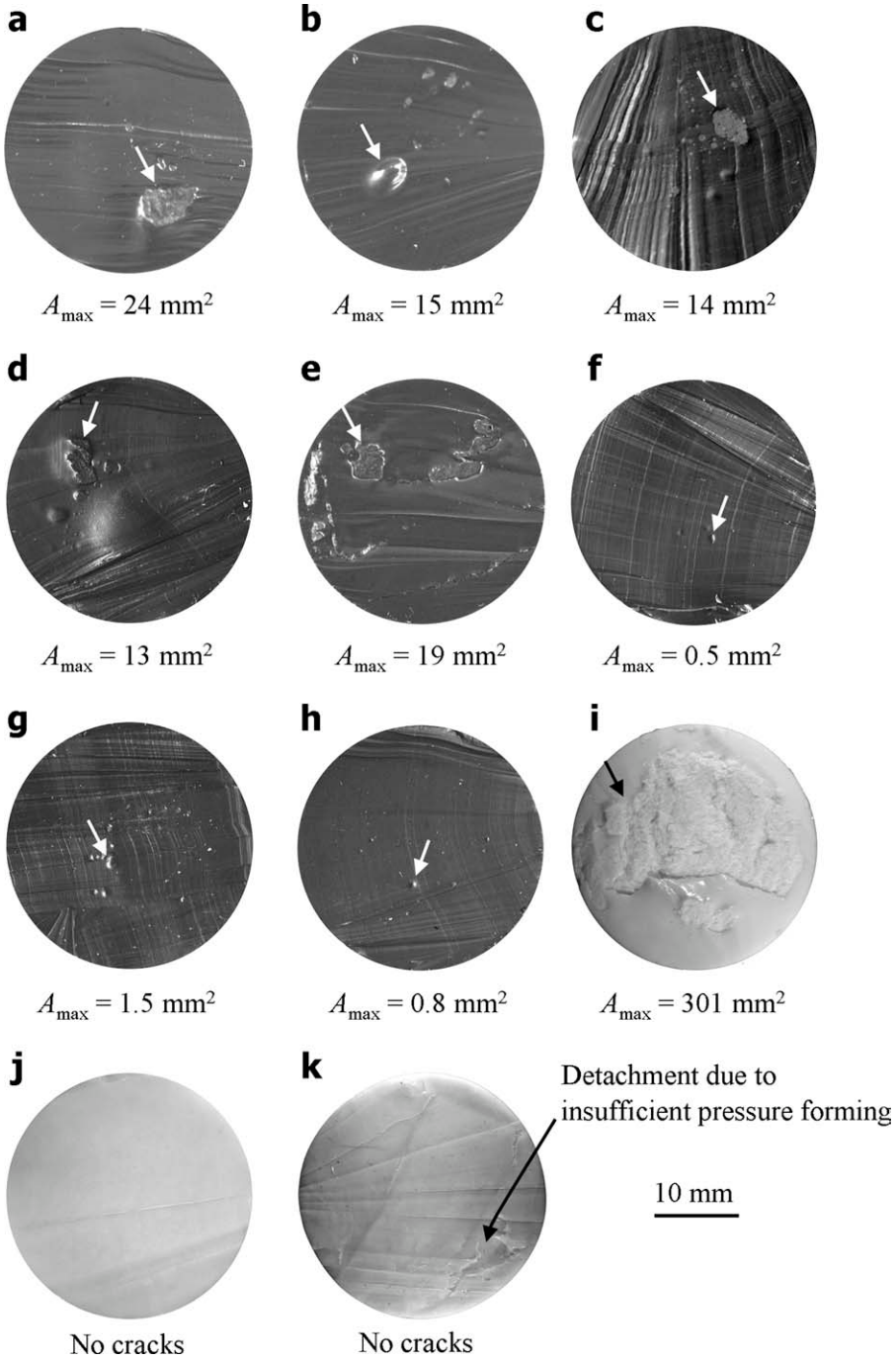


**Figure 7** Optical microscope images of cracks in cut specimens: (a) N110-25, (b) N220-25, (c) N330-25, (d) N550-25, (e) N774- 25, (f) N110-50, (g) N330-50, (h) N774-50, (i) NF, (j) SC-30, and (k) SC-60

influenced by primary particle size and became slighter when the CB content became higher. In contrast, no cracks were observed in the SC-filled rubbers.

### SEM observation of fracture surfaces

Figure 8 shows SEM images of fracture origins of EPDM rubber containing 25 phr of CB N330 (N330-25). Figure 8(a) shows the fracture surface with a defect of 80 μm in size. Figure 9(a) shows element images of the defect shown in Figure 8(a-1) of N330-25 obtained by EDX (energy dispersive X-ray spectrometry). As the elements of this defect did not show any differences to those of the other regions, the type of the defect could not be identified. Although a defect of 25 μm in size, which was composed of aluminum and oxygen as shown in Figure 9(b), was also observed on the facture surface as shown in Figure 8(a-3), the fracture did not occur from this defect.

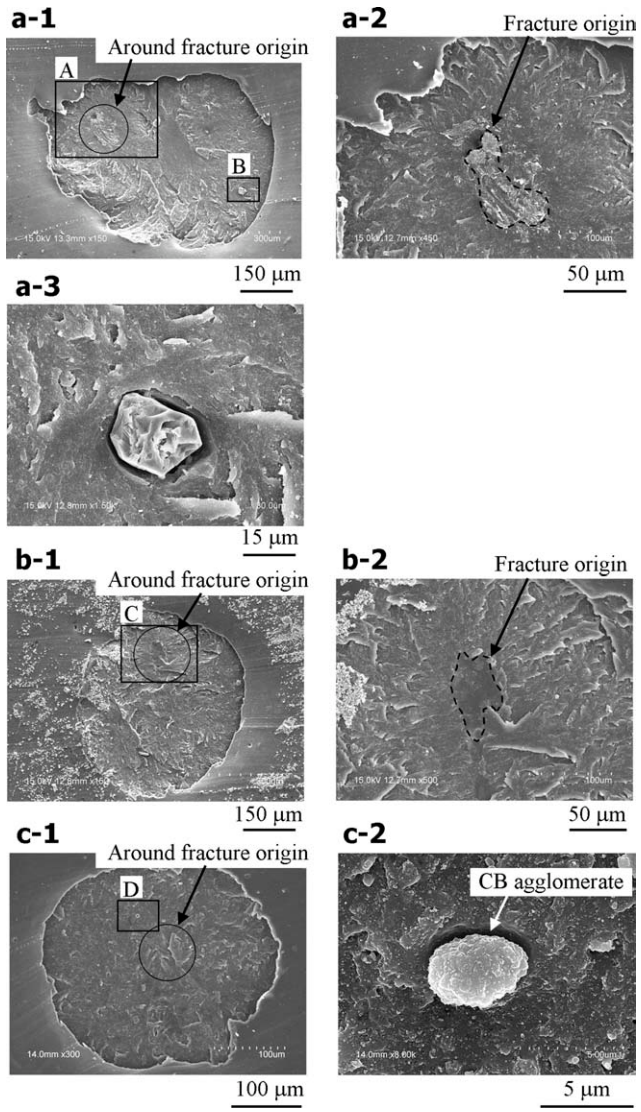


**Figure 8** SEM images of fracture surfaces of N330-25: (a) fracture with defect, (a-1) low magnification, (a-2) magnification of A, (a-3) magnification of B, (b) fracture with facet, (b-1) low magnification, (b-2) magnification of C, (c) fracture without anything, (c-1) low magnification, and (c-2) magnification of D.

Figure 8(b) shows the fracture surface with a flat area (facet) of 70 μm. Figure 10 shows the element images of this facet by EDX. There were no differences between the facet and the other regions in terms of elements. From our previous study using AFM,[22] it was inferred that submicrometer-sized low-strength structure exists in a matrix of EPDM rubber, and nanoscale fractures caused by bubbles formed from solute hydrogen molecules originates from the low-strength site, which is believed to be formed in relation to the inhomogeneity of the cross-link density. The facet is considered to be not so much an extrinsic defect as such a low-strength site.

Figure 8(c) shows the fracture surface without anything. It is considered that the fracture shown in Figure 8(c) also originated from the low-strength site as well as that in Figure 8(b). Although a CB agglomerate of 5 μm can be seen on the fracture surface shown in Figure 8(c), the fracture did not occur from this CB agglomerate.

Figure 11 shows SEM images of fracture surfaces of EPDM rubber containing 25 phr of CB N774 (N774-25). Figure 11(a) shows the fracture surface with a defect of 80 μm in size. Figure 12(a) shows element images of this defect by EDX. Sulfur and zinc were detected, while carbon was mainly detected in the matrix. For vulcanization, sulfur and zinc oxide (ZnO) were added to a rubber. The defect shown in Figure 11(a-2) is considered to be a cluster formed in relation to the sulfur and zinc oxide.

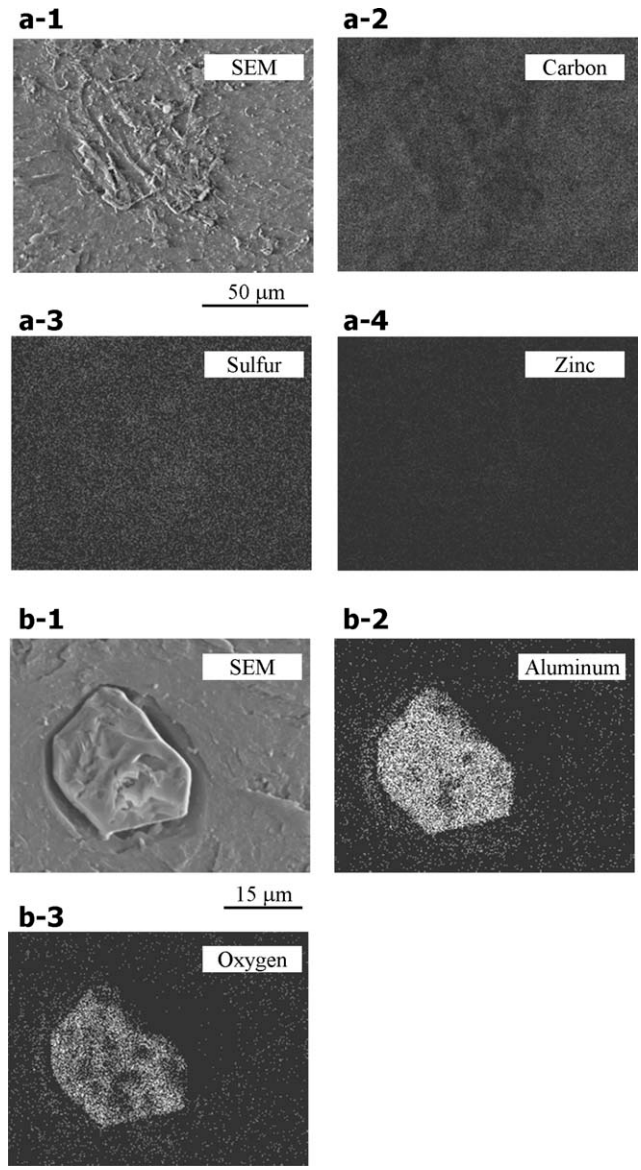


**Figure 9** EDX images of areas A and B of N330-25: (a) area A, (a-1) SEM, (a-2) carbon, (a-3) sulfur, (a-4) zinc, (b) area B, (b-1) SEM, (b-2) aluminum, and (b-3) oxygen.

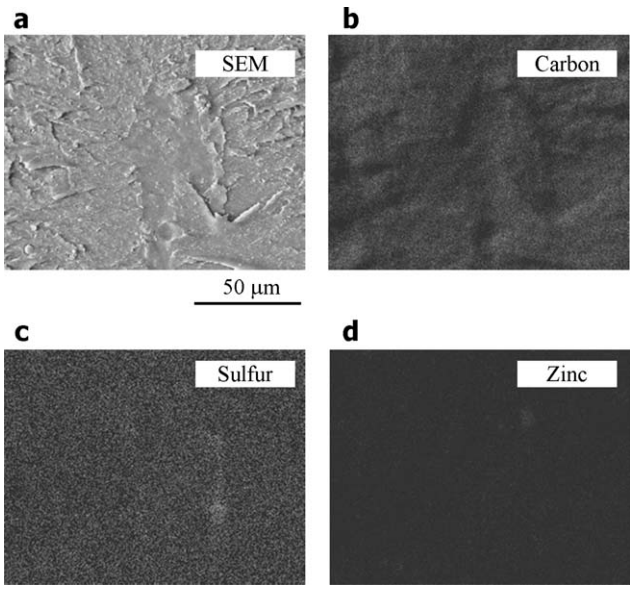


**Figure 10** EDX images at area C of N330-25: (a) SEM, (b) carbon, (c) sulfur, and (d) zinc.

Figure 11(b) shows a fracture surface with a facet of 50 μm. It is believed that this fracture originated from the low-strength site mentioned in Figure 8(b,c). Although a cluster composed of sulfur and zinc of 25 μm in size was observed on the fracture surface as shown in Figures 11(b-2) and 12(b), the fracture did not occur from this cluster.

Table IV shows the types of fracture origins of EPDM rubbers (N110-25, N220-25, N330-25, N550-25, N774-25, and N330-50). Ten fracture surfaces were observed for the 25 phr CB-filled rubbers, and

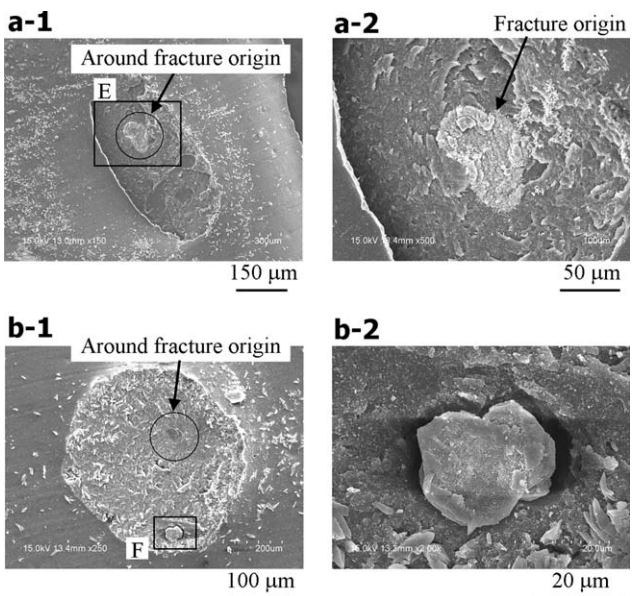


**Figure 11** SEM images of fracture surfaces of N774-25: (a) fracture with defect, (a-1) low magnification, (a-2) magnification of E, (b) fracture with facet, (b-1) low magnification, and (b-2) magnification of F.

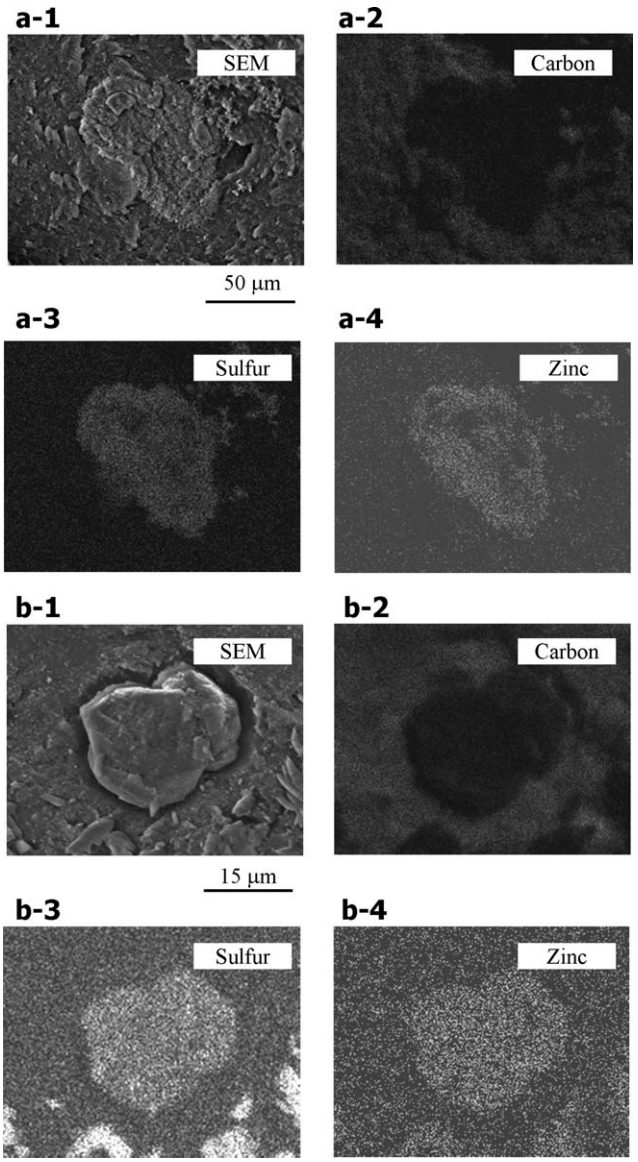


**Figure 12** EDX images of areas E and F of N774-25: (a) area E, (a-1) SEM, (a-2) carbon, (a-3) sulfur, (a-4) zinc, (b) area F, (b-1) SEM, (b-2) carbon, (b-3) sulfur, and (b-4) zinc.

five fracture surfaces were observed for N330-50. The facture origins can be divided into three types: nothing or facet, cluster with sulfur and zinc, and (extrinsic) defect. In this study, the nothing or facet and cluster with sulfur and zinc are regarded as intrinsic defects. It is inferred that the fracture originates from the maximum size defect, irrespective of the type of defects. The maximum defect sizes of these rubbers did not show a big difference and ranged from 70 to 90 μm.

### Influences of material strength and hydrogen permeation properties on crack damage

In our previous studies,[11–13] it was assumed that internal cracks were initiated as a result of the stress

**TABLE IV**
**Types of Fracture Origin of CB-Filled Rubbers by Scanning Electron Microscopy**

| Type of fracture origin | N110–25 | N220–25 | N330–25 | N550–25 | N774–25 | N330–50 |
|---|---|---|---|---|---|---|
| Nothing or facet | | | | | | |
| Number | 9 | 6 | 8 | 7 | 7 | 5 |
| Maximum size (μm) | 90 | 50 | 70 | 80 | 50 | 70 |
| Cluster with S and Zn | | | | | | |
| Number | 1 | 3 | 0 | 1 | 2 | 0 |
| Maximum size (μm) | 50 | 70 | – | 60 | 80 | – |
| Extrinsic defect | | | | | | |
| Number | 1 | 1 | 2 | 2 | 1 | 0 |
| Maximum size (μm) | 50 | 60 | 80 | 50 | 60 | – |

concentration of bubbles formed by dissolved hydrogen molecules after decompression. To estimate the critical hydrogen pressure at crack initiation ($p_F$), the shape of the bubbles was regarded as disc-like, and its tearing energy ($T$) was calculated by the finite element method. Static crack growth tests[23–25] were also conducted, and the threshold tearing energy of the static crack ($T_{s,\mathrm{th}}$) was evaluated. The condition of crack initiation can be written as follows:

$$T \geq T_{s,\mathrm{th}} \tag{12}$$

The internal pressures at crack initiation ($\Pi_F$) of NFP, NF, SCP, and CBP were calculated in the previous study.[11–13] Table V shows the results obtained in Ref. [13]. The values of $\Pi_F$ and $p_F$ were expressed based on atmospheric pressure (0.1 MPa), that is, gage pressure. If the internal pressure in the bubbles ($\Pi$) is assumed to be equal to applied hydrogen pressure ($p$) for hydrogen exposure, the critical hydrogen pressures ($p_F$) can be successfully estimated in terms of the critical internal pressure ($\Pi_F$), as $\Pi_F$ showed good coincidence with $p_F$ for NFP, NF, and SCP.

In contrast, the $p_F$ value of CBP was overestimated by this method, because $\Pi_F$ was twice as large as $p_F$. As CBP contains CB as a filler, a lot of hydrogen was absorbed in the rubber compared with the other rubbers. This absorbed hydrogen raises the hydrogen concentration of CBP. Because the increase of $\Pi$ originated from the absorbed hydrogen by CB in CBP was underestimated, it was inferred that $p_F$ was smaller than $\Pi_F$. Therefore, it is supposed that $\Pi > p$ for CB-filled rubbers, that is, the rubber experienced more pressurization due to additional hydrogen.

In this study, the maximum principal stress criterion was applied as a more simplified estimation of the $\Pi_F$ value because the threshold tearing energies for static cracking of all the rubbers have not yet been obtained. In this investigation, the shape of the bubbles was regarded as being spherical, and it was assumed that internal cracks initiated when the maximum tangential stress ($\sigma_{\theta,\max}$) exceeded true tensile strength ($\sigma_T$). When rubbers follow the polynominal Mooney–Rivlin model shown in eq. (1), the internal pressure ($\Pi$) and maximum tangential stress ($\sigma_{\theta,\max}$) are expressed as follows[14,26]:

$$\Pi = (5 - \frac{1}{\lambda_1^4} - \frac{4}{\lambda_1})C_{10} - 2(1 + \frac{1}{\lambda_1^2} - 2\lambda_1)C_{01} - (\frac{177}{5} + \frac{1}{\lambda_1^8} + \frac{8}{5\lambda_1^5} - \frac{6}{\lambda_1^4} + \frac{8}{\lambda_1^2} - \frac{24}{\lambda_1} - 16\lambda_1)C_{20} \tag{13}$$

$$\sigma_{\theta,\max} = (-5 - \frac{1}{\lambda_1^4} + \frac{4}{\lambda_1} + 2\lambda_1^2)C_{10} + 2(1 - 2\lambda_1 + \lambda_1^4)C_{01} + (\frac{177}{5} - \frac{3}{\lambda_1^8} + \frac{8}{5\lambda_1^5} + \frac{6}{\lambda_1^4} + \frac{4}{\lambda_1^2} - \frac{24}{\lambda_1} - 16\lambda_1 - 12\lambda_1^2 + 8\lambda_1^4)C_{20} \tag{14}$$

where $\lambda_1$ is the tangential stretch at the inner surface of the spherical bubble. Figure 13 shows the fitted nominal stress–stretch curves of N110-50 and N774-25 by eq. (1). Table VI shows the material constants obtained by fitting. The true tensile strength ($\sigma_T$) was Conveniently calculated under incompressibility as follows:

**TABLE V**
**Estimation of Internal Pressure at Crack Initiation of Unfilled, SC-Filled, and CB-Filled Rubbers**

| Materials | $p_F$ (MPa) | Bubble size (μm) | $T_{s,\mathrm{th}}$ (N/m) | $\Pi_F$[a] (MPa) |
|---|---|---|---|---|
| Unfilled and peroxide-crosslinked EPDM, NFP | 1.0–1.5 | 20 | 50 | 1.137 |
| Unfilled and sulfur-vulcanized EPDM, NF | 1.5–2.0 | 20 | 100 | 1.551 |
| SC-filled and peroxide-crosslinked EPDM, SCP | 4.0–4.5 | 45 | 220 | 4.287 |
| CB-filled and peroxide-crosslinked EPDM, CBP | 4.0–5.0 | 20 | 950 | 8.993 |

[a] The values of $p_F$ and $\Pi_F$ were expressed based on gage pressure.

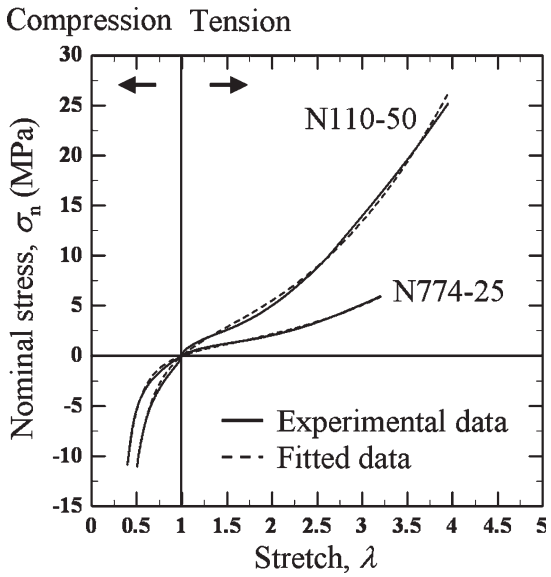


**Figure 13** Estimation of material constants from nominal stress–stretch curves of N110-50 and N774-25.

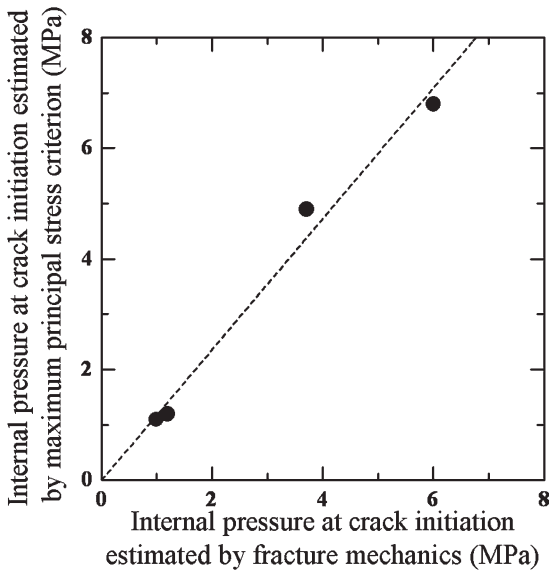


**Figure 14** Comparison of calculated internal pressures at crack initiation between fracture mechanics and maximum principal stress criteria.

$$\sigma_T = \sigma_{nF}\lambda_F \tag{15}$$

where $\sigma_{nF}$ is the nominal tensile strength and $\lambda_F$ is the fracture stretch. The mean $\sigma_{nF}$ and $\lambda_F$ values of two specimens were used for calculation of the true tensile strength. Figure 14 shows the comparison of the $\Pi_F$ values of NFP, NF, SCP, and CBP obtained by the fracture mechanics and maximum principal stress criteria. As the maximum defect size was about 80 μm from SEM observations, the $\Pi_F$ values when the bubble size was 80 μm were calculated using the fracture mechanics criterion. As the $\Pi_F$ values increases when the mechanical properties of the rubbers are improved, the $\Pi_F$ values of the filled rubbers are higher than those of the unfilled rubbers. The $\Pi_F$ values obtained from the fracture mechanics criterion were nearly proportional to those obtained from the maximum principal stress criterion, although these values did not show a good agreement. Therefore, a relative comparison of the $\Pi_F$ values can be conducted by the maximum principal stress criterion. Furthermore, it was assumed that $c_0$ ($=Sp$) $\propto \Pi$ conveniently since the internal pressure ($\Pi$) is considered to be higher than the hydrogen pressure ($p$) for the CB-filled rubbers from the result of Table V; then, the relationship among crack damage, hydrogen gas solubility, and mechanical properties of the EPDM rubbers.

**TABLE VI**
**Material Constants of Unfilled, SC-Filled, and CB-Filled Rubbers**

| Materials | Material constants (MPa) | | |
|---|---|---|---|
| | $C_{10}$ | $C_{01}$ | $C_{20}$ |
| N110–25 | 0.541 | 0.072 | 0.048 |
| N220–25 | 0.565 | 0.058 | 0.043 |
| N330–25 | 0.622 | 0.029 | 0.035 |
| N550–25 | 0.594 | 0.063 | 0.037 |
| N774–25 | 0.430 | 0.133 | 0.030 |
| N110–50 | 1.206 | 0.093 | 0.082 |
| N330–50 | 1.394 | 0.015 | 0.084 |
| N774–50 | 0.722 | 0.175 | 0.056 |
| NF | 0.292 | 0.060 | – |
| SC-30 | 0.437 | 0.016 | 0.006 |
| SC-60 | 1.178 | 0.218 | 0.014 |

Figure 15 shows the relationship among the degree of crack damage, internal pressure at crack initiation ($\Pi_F$), and hydrogen solubility ($S$) of the unfilled, SC-filled, and CB-filled rubbers. Hydrogen gas solubility ($S$) is regarded as the driving force for crack formation, while the critical internal pressure at crack initiation ($\Pi_F$) is regarded as the resistance to crack formation. The degree of crack damage was evaluated in terms of the square root of the maximum crack area $(A_{max})^{1/2}$. We refer to $(A_{max})^{1/2}$ as the maximum crack length ($a_{max}$), whose dimension is in mm. The $a_{max}$ value calculated from the largest $A_{max}$ value is shown in Figure 15. In these figures, the $a_{max}$ value should increase as the $S$ value became larger and the $\Pi_F$ value became smaller; the value of $\Pi_F$ increases in turn as the values of tensile elastic modulus ($E$) and true fracture strength ($\sigma_T$) increase for each rubber. The $a_{max}$ values tended to become larger with an increase in the $S$ values and a decrease in the $\Pi_F$ values. To evaluate the influence of the hydrogen gas solubility ($S$) and the estimated internal pressure at crack initiation ($\Pi_F$) relating to material strength more quantitatively,

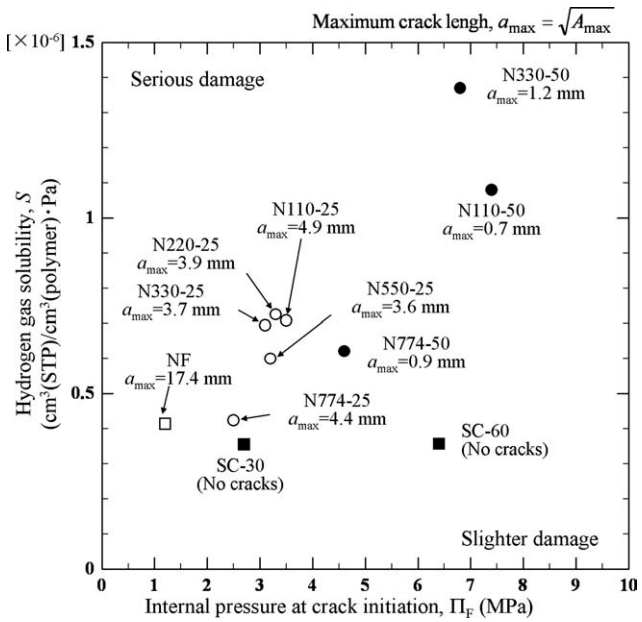


**Figure 15** Relationship among crack damage, hydrogen gas solubility, and internal pressure at crack initiation.

the relationship between the maximum crack length ($a_{max}$) and the ratio of $S$ to $\Pi_F$ ($S/\Pi_F$) was evaluated.

Figure 16 shows the relationship between the maximum crack length ($a_{max}$) and ratio of $S$ to $\Pi_F$ ($S/\Pi_F$). The mean value and range of $a_{max}$ are shown by material. The $a_{max}$ values approximately became larger as the $S/\Pi_F$ values became larger. As the SC-filled rubbers (SC-30 and SC-60) have relatively smaller $S/\Pi_F$ values, it is inferred that the crack damage was slighter than that of the other rubbers (unfilled and CB-filled rubbers). The reason the crack damage of NF was the most serious was because the $S/\Pi_F$ value was the largest of all the rubbers. As the CB-filled rubbers have relatively higher $S/\Pi_F$ values compared with SC-filled rubbers, the crack damage was more serious than those of the SC-filled rubbers, although the $\Pi_F$ values were comparable. A smaller CB particle increases the solubility of rubbers, while at the same time it reinforces the rubbers and increases the $\Pi_F$ value; consequently, the $S/\Pi_F$ values are hardly influenced by primary particle size. Therefore, it is inferred that the crack damage in the CB-filled rubbers was not influenced by the primary particle size of the CB.

## CONCLUSIONS

Five types of CB (ASTM N110, N220, N330, N550, and N744) were selected, and eight filled EPDM rubbers were manufactured by varying the added amount and types of CB. Hydrogen permeation and high-pressure hydrogen exposure tests of the rubbers were conducted; then, the influence of CB on hydrogen permeation properties and crack damage was investigated. The results obtained can be summarized as follows:

1. As for the nitrogen and hydrogen absorptions of the filler powders, when $N_2$ specific surface area became larger, the hydrogen absorption amount also increased. The hydrogen absorption of SC was higher than that of CB.
2. While the hydrogen gas permeability ($Q$) of filled rubbers was hardly influenced by the $N_2$ specific surface area of the CB, the hydrogen gas diffusivity ($D$) and solubility ($S$) were clearly influenced. The $D$ values of the CB-filled rubbers became smaller and the $S$ value became larger, when the $N_2$ specific surface area became larger. This is considered to be because hydrogen molecules absorbed by the CB participated in hydrogen diffusion.
3. The $S$ values of the CB-filled rubbers were larger than those of SC-filled rubbers, although the $N_2$ specific surface area of the SC was larger than that of CB. It is inferred that the interface structure between matrix and filler strongly influences the solubility of the filled rubbers.
4. Crack damage was evaluated in terms of the maximum crack length on the cross-section of specimens ($a_{max}$). The hydrogen gas solubility ($S$) was assumed to be proportional to the internal pressure in the bubbles ($\Pi$) and was regarded as the driving force for crack initiation. Furthermore, the critical hydrogen

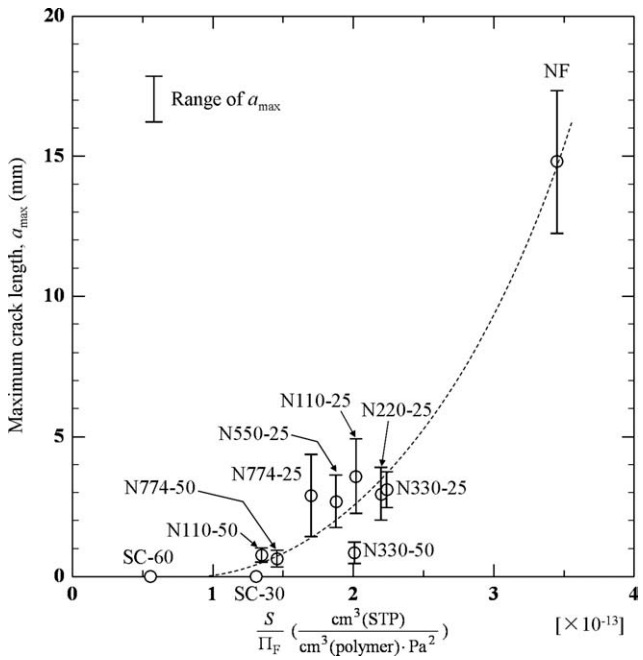


**Figure 16** Relationship between maximum crack length and ratio of hydrogen gas solubility to estimated internal pressure at crack initiation.

pressure at crack initiation ($\Pi_F$) was calculated using the maximum principal stress criterion and was regarded as the resistance to crack formation. As a result, the value of $a_{max}$ became larger when the ratio of $S$ to $\Pi_F$ ($S/\Pi_F$) became larger. As the $\Pi_F$ value increases with an increase in tensile elastic modulus ($E$) and true fracture strength ($\sigma_T$) of the rubbers, both the hydrogen gas solubility and mechanical properties such as $E$ and $\sigma_T$ influenced crack damage.

5. The crack damage in the CB-filled rubbers was not influenced by the primary particle size. This is considered to be because a smaller CB particle increases the hydrogen gas solubility of the rubbers, while at the same time it reinforces the rubbers, that is, the $S/\Pi_F$ value was hardly influenced by the particle size of the CB.

This research was supported by the NEDO project "Fundamental Research Project on Advanced Hydrogen Science (2006–2012)." The authors thank Mr. Y. Izumi and Ms. R. Ayaka for obtaining such useful results. The rubbers were manufactured by Takaishi-Industry Co.

## References

1. Briscoe, B. J.; Savvas, T.; Kelly, C. T. Rubber Chem Technol 1994, 67, 384.
2. Gent, A. N.; Tompkins, D. A. J Appl Phys 1969, 40, 2520.
3. Gent, A. N.; Lindley, P. B. Proc R Soc A 1958, 249, 195.
4. Lindsey, G. H. J Appl Phys 1967, 38, 4843.
5. Stevenson, A.; Glyn, M. Rubber Chem Technol 1995, 68, 197.
6. Stewart, C. W. J Polym Sci A 1970, 8, 937.
7. Zakaria, S.; Bricoe, B. J. Chemtech 1990, 20, 492.
8. Ender, D. H. Chemtech 1986, 16, 52.
9. Briscoe, B. J.; Liatsis, D. Rubber Chem Technol 1992, 65, 350.
10. Epstein, P. S.; Plesset, M. S. J Chem Phys 1950, 18, 1505.
11. Yamabe, J.; Nishimura, S. Trans J Soc Mech Eng A 2009, 75, 633.
12. Yamabe, J.; Nishimura, S. Trans J Soc Mech Eng A 2009, 75, 1727.
13. Yamabe, J.; Nishimura, S. Proc of the 18th European Conference on Fracture, CD-ROM, Dresden, Germany, 2010.
14. Yamabe, J.; Nishimura, S. Int J Hydrogen Energy 2009, 34, 1977.
15. Yamabe, J.; Matsumoto, T.; Nishimura, S. Polym Test 2011, 30, 76.
16. Tokai Carbon Co., Ltd. Physicochemical properties of carbon black, http://www.tokaicarbon.co.jp/en/products/carbon_b/seast/index.html, 2011. Accessed on April 28, 2011.
17. Motoyama, M.; Hashizume, G. Bull Chem Soc Jpn 1972, 45, 38.
18. Treloar, L. R. G. The Physics of Rubber Elasticity; Oxford University Press: London, 2005.
19. Brunauer, S.; Emmett, P. H.; Teller, E. J Am Chem Soc 1938, 60, 309.
20. Van Amerongen, G. J. Rubber Chem Technol 1964, 37, 1067.
21. Langumuir, I. J Am Chem Soc 1918, 40, 1361.
22. Yamabe, J.; Nishimura, S. J Mater Sci 2011, 46, 2300.
23. Thomas, A. G. J Appl Polym Sci 1960, 8, 168.
24. Lake, A. J.; Lindley, P. B. J Appl Polym Sci 1964, 8, 707.
25. Yamabe, J.; Nishimura, S. Trans J Soc Mech Eng A 2009, 75, 1531.
26. Green, A. E.; Zerna, W. Theoretical Elasticity; Oxford University Press: London, 1954.